



Pulsed oxygenation events drove progressive oxygenation of the early Mesoproterozoic ocean

Jin Luo^a, Xiaoping Long^{a,*}, Fred T. Bowyer^b, Benjamin J.W. Mills^b, Jie Li^c, Yijun Xiong^b, Xiangkun Zhu^d, Kan Zhang^e, Simon W. Poulton^b

^a State Key Laboratory of Continental Dynamics, Department of Geology, Northwest University, Xi'an 710069, China

^b School of Earth and Environment, University of Leeds, Leeds, LS2 9JT, UK

^c State Key Laboratory of Isotope Geochemistry, Guangzhou Institute of Geochemistry, Chinese Academy of Sciences, Guangzhou 510640, China

^d MNR Key Laboratory of Isotope Geology, MLR Key Laboratory of Deep-Earth Dynamics, Institute of Geology, Chinese Academy of Geological Sciences, Beijing, China

^e State Key Laboratory of Marine Environmental Science, Xiamen University, Xiamen 361005, China

ARTICLE INFO

Article history:

Received 17 July 2020

Received in revised form 30 December 2020

Accepted 6 January 2021

Available online 26 January 2021

Editor: F. Moynier

Keywords:

Mesoproterozoic

palaeoredox

Fe speciation

molybdenum isotopes

ocean oxygenation

ABSTRACT

The Mesoproterozoic era has long been considered a time of relative environmental and biological stasis. However, emerging insight suggests that this period may have been more dynamic than previously considered, both in terms of oxygenation and potential consequences for biological evolution. Nevertheless, our understanding of this immense period of time remains limited. To provide more detailed constraints on oxygenation dynamics, we report a multiproxy geochemical study of an early Mesoproterozoic (~1600–1540 million years ago, Ma) carbonate-dominated succession from the North China craton. We include inorganic carbon isotope ($\delta^{13}\text{C}_{\text{carb}}$), iron-speciation, and major and trace element data, in addition to molybdenum isotopic compositions ($\delta^{98/95}\text{Mo}$). These geochemical data support previous inferences of persistent anoxic and ferruginous deeper water conditions in the earliest Mesoproterozoic ocean, with limited oxygenation of surface waters. However, the behaviour of these redox-sensitive geochemical proxies reveals pulsed oxygenation events, with each event increasing the maximum depth of oxygenation, leading to overall progressive oxygenation of the ocean. During these pulsed oxygenation events we find the lightest Mo isotope signatures ever measured in the rock record, which we attribute to initial drawdown of isotopically light Mo in association with extensive Mn and Fe (oxyhydr)oxide precipitation, followed by diagenetic recycling. However, shallower water sediments deposited after the pulses of deeper water oxygenation more faithfully record the Mo isotopic composition of coeval seawater. For these samples, we utilise a single reservoir Mo cycling model, constrained by an updated estimate of Mesoproterozoic seawater Mo concentration, and scaled using a function associated with differential organic carbon flux between the shelf and basin. When scaled to modern rates of Mo accumulation under variable marine redox conditions, our modelling estimates suggest a minimum oxic seafloor area of ~30% of the total seafloor area at ~1540 Ma. It remains unclear whether the oxygenation observed across this ~60 million year interval represents a progressive transition to a more persistently oxygenated ocean, or whether oceanic oxygen levels fluctuated considerably through the later Mesoproterozoic.

© 2021 Elsevier B.V. All rights reserved.

1. Introduction

The Mesoproterozoic (1.6–1.0 Ga) has long been considered an interval of relative geochemical and evolutionary stasis (e.g., Buick et al., 1995; Javaux and Lepot, 2018), and although atmospheric oxygen levels are highly debated (Cole et al., 2016; Zhang et al., 2016; Canfield et al., 2018), oxygen concentrations are commonly

considered to have stabilised at a low to moderate level (<1% to >4% of the present atmospheric level; PAL). However, on closer inspection, individual Mesoproterozoic marine basins reveal significant variability in carbonate carbon ($\delta^{13}\text{C}_{\text{carb}}$) isotopes (e.g., Chu et al., 2007; Gilleaudeau and Kah, 2013; Zhang et al., 2018) and regional redox conditions, which may, or may not, be linked to fluctuations in atmospheric oxygen (e.g., Zhang et al., 2016; Beghin et al., 2017), in addition to hitherto unrecognised diversity in Mesoproterozoic complex multicellularity (e.g., Zhu et al., 2016; Beghin et al., 2017).

* Corresponding author.

E-mail address: longxp@nwnu.edu.cn (X. Long).

Available geochemical evidence points to redox stratification in the Mesoproterozoic ocean, with anoxic deeper waters overlain by shallower oxic waters (e.g., Scott et al., 2008; Planavsky et al., 2011; Poulton and Canfield, 2011; Doyle et al., 2018), although suboxic deeper waters (Slack et al., 2007; Slack and Cannon, 2009) and variable redox conditions (Planavsky et al., 2018) have also been suggested. When anoxic, deeper oceans are thought to have been dominantly ferruginous, with euxinia restricted to some productive continental margins (Scott et al., 2008; Planavsky et al., 2011; Poulton and Canfield, 2011; Doyle et al., 2018). However, the extent of ocean oxygenation remains particularly poorly constrained. A low resolution study spanning ~1.6–0.8 Ga marine sediments from the Southern Urals found evidence for restriction of oxygenated waters to only very shallow marine settings (Doyle et al., 2018). By contrast, studies from other localities suggest that the earlier Mesoproterozoic ocean may have witnessed pulsed oxygenation events (Zhang et al., 2018; Shang et al., 2019), as well as potential intervals of oxygen minimum zone (OMZ)-type conditions overlying fully oxygenated deeper waters, the earliest potential evidence for which currently comes from the ~1.4 Ga Xiamaling Formation on the North China Craton (Zhang et al., 2016, 2019).

The early Mesoproterozoic carbonate-dominated Gaoyuzhuang Formation (~1.60–1.54 Ga) of the North China Craton has received particular attention, due to the concurrent appearance of decimetre-scale, multicellular eukaryotic macrofossils (Zhu et al., 2016) with geochemical evidence for enhanced oxygenation of the marine environment (Zhang et al., 2018; Shang et al., 2019; Wang et al., 2020). However, the global extent of this inferred oxygenation remains uncertain, and it is also unclear whether the Gaoyuzhuang Formation records a single transient oxygenation event contemporaneous with the Gaoyuzhuang fossils, or whether the initial oxygenation event marked the onset of more pervasive longer-term oxygenation (cf., Zhang et al., 2018; Shang et al., 2019).

To address these issues we present a multi-proxy geochemical dataset for the Gaoyuzhuang Formation, with a specific focus on identifying both regional and global marine redox conditions. Our dataset incorporates major and trace element concentrations, Fe speciation, and total organic carbon (TOC) measurements, in addition to carbonate C ($\delta^{13}\text{C}_{\text{carb}}$) and Mo ($\delta^{98}\text{Mo}$) isotope analyses. For Mo in particular, a long oceanic residence time (~800 ky; Morford and Emerson, 1999) results in globally uniform Mo concentrations and Mo isotopic compositions in the modern ocean. Therefore, although the residence time would have been less in ancient anoxic oceans, changes in seawater Mo isotopic composition are considered to reflect changes in the global Mo budget, which in turn are intrinsically linked to changes in seawater palaeoredox conditions (e.g., Siebert et al., 2003; Asael et al., 2018). Palaeoredox studies employing Mo isotope systematics have classically targeted shales that show independent evidence for deposition beneath locally euxinic water column conditions, in order to reconstruct the Mo isotopic composition of global seawater, which is intimately associated with the relative proportion of oxic versus anoxic (and specifically euxinic) seafloor area (e.g., Kendall et al., 2011; Dahl et al., 2010). Here, we utilise the Mo isotopic composition of carbonates to determine seawater $\delta^{98}\text{Mo}$ (Voegelin et al., 2010; Thoby et al., 2019), by first screening our samples for those that appear to record negligible isotopic fractionation during the incorporation of molybdate into the carbonate lattice. We then use a single reservoir Mo cycling model to provide the first semi-quantitative constraints on the global extent of ocean oxygenation at ~1.54 Ga. Our combined approach provides evidence for multiple oxygenation events in the early Mesoproterozoic ocean, and gives new insight into the role of pulsed oxygenation events in driving progressive oxygenation across this dynamic interval.

2. Geological background

The Yanliao basin developed during a series of long-lived extensional events following the Paleoproterozoic amalgamation of the North China Craton. An ~9 km thick late Paleo- to Neoproterozoic sedimentary succession was deposited close to the depositional centre of the Yanliao basin in the Jixian area (Fig. 1), and comprises the Paleoproterozoic Changcheng Group (~1.66–1.60 Ga), including the Changzhougou, Chuanlinggou, Tuanshanzi and Dahongyu formations; the Mesoproterozoic Jixian Group (~1.60–1.40 Ga), including the Gaoyuzhuang, Yangzhuang, Wumishan, Hongshuizhuang and Tieling formations; an unnamed group (~1.40–1.36 Ga), that includes the Xiamaling Formation; and the unconformably overlying Neoproterozoic Qingbaikou Group (~1.00–0.78 Ga), including the Changlongshan and Jing'eryu formations (Fig. 1; Lu et al., 2008).

The carbonate-dominated Gaoyuzhuang Formation is the lowermost formation of the Jixian Group, and was deposited unconformably upon the Dahongyu Formation of the Changcheng Group (Chen et al., 1981; Lu et al., 2008). The Gaoyuzhuang Formation has a maximum depositional age of ~1.6 Ga based on SHRIMP U-Pb zircon ages from volcanics in the underlying Dahongyu Formation (Lu et al., 2008). In Jixian county, the Gaoyuzhuang Formation is >1500 m thick and dominated by littoral to neritic carbonate facies with rare clastic interbeds, and was deposited in a stable epicontinental sea inferred to have been openly connected to the global ocean (Chen et al., 1981; Chu et al., 2007). In the Jixian area the Gaoyuzhuang Formation has been subdivided into four lithological members based on sedimentology and inferred shallowing-upward sequences (Fig. 2; Mei, 2007; Guo et al., 2013; Zhang et al., 2018).

Member I is characterised by ripple-marked shoreface sandstones that give way to cherty dolomicrite with intercalated clay-rich and stromatolitic dolomicrite in the middle to upper part (Fig. 2), suggesting a change in facies from supratidal to intertidal deposition. The lower part of Member II dominantly consists of thin, planar beds of Mn-rich dolomicrite, which transition to subtidal massive dolosparite. The boundary between members II and III is marked by a decimetre-scale interval of medium bedded nodular limestone with muddy limestone and minor shale interbeds at the base. The lower part of Member III records a regional marine transgression from shallow subtidal to deeper outer shelf conditions, close to (or possibly below) storm wave base (Mei, 2007; Guo et al., 2013). Massively bedded carbonates, including limestone with molar tooth structure and columnar stromatolites in upper Member III suggest marine regression and a return to subtidal deposition (Mei, 2007). Member IV comprises coarse-grained stromatolitic dolostone, interbedded with bituminous dolostone and an overlying unit of dolomicrite with cherty concretions, interpreted to represent a subtidal to intertidal depositional environment. The metamorphic grade of Gaoyuzhuang strata (in the Yanliao Basin specifically) is below prehnite-pumpellyite facies (Chu et al., 2007; Wang et al., 2020).

Decimetre-scale multicellular fossils, displaying an unusual degree of morphological complexity for Mesoproterozoic macrofossils, have been documented from the middle of Member III in the Kuancheng and Qianxi areas to the east of Jixian County (Zhu et al., 2016). A tuff deposit intercalated with sediments of lower Member III in Jixian County yielded a zircon U-Pb (LA-ICP-MS) age of 1577 ± 12 Ma (Tian et al., 2015), and zircon U-Pb ages of 1560 ± 5 Ma (LA-ICP-MS) and 1559 ± 12 Ma (SHRIMP) have also been reported from a tuff bed in upper Member III in Yanqing County (Li et al., 2010). Together with the maximum depositional age derived from the Dahongyu Formation volcanics, this constrains deposition of the Gaoyuzhuang Formation, and associated fossils, from ~1.60–1.54 Ga.

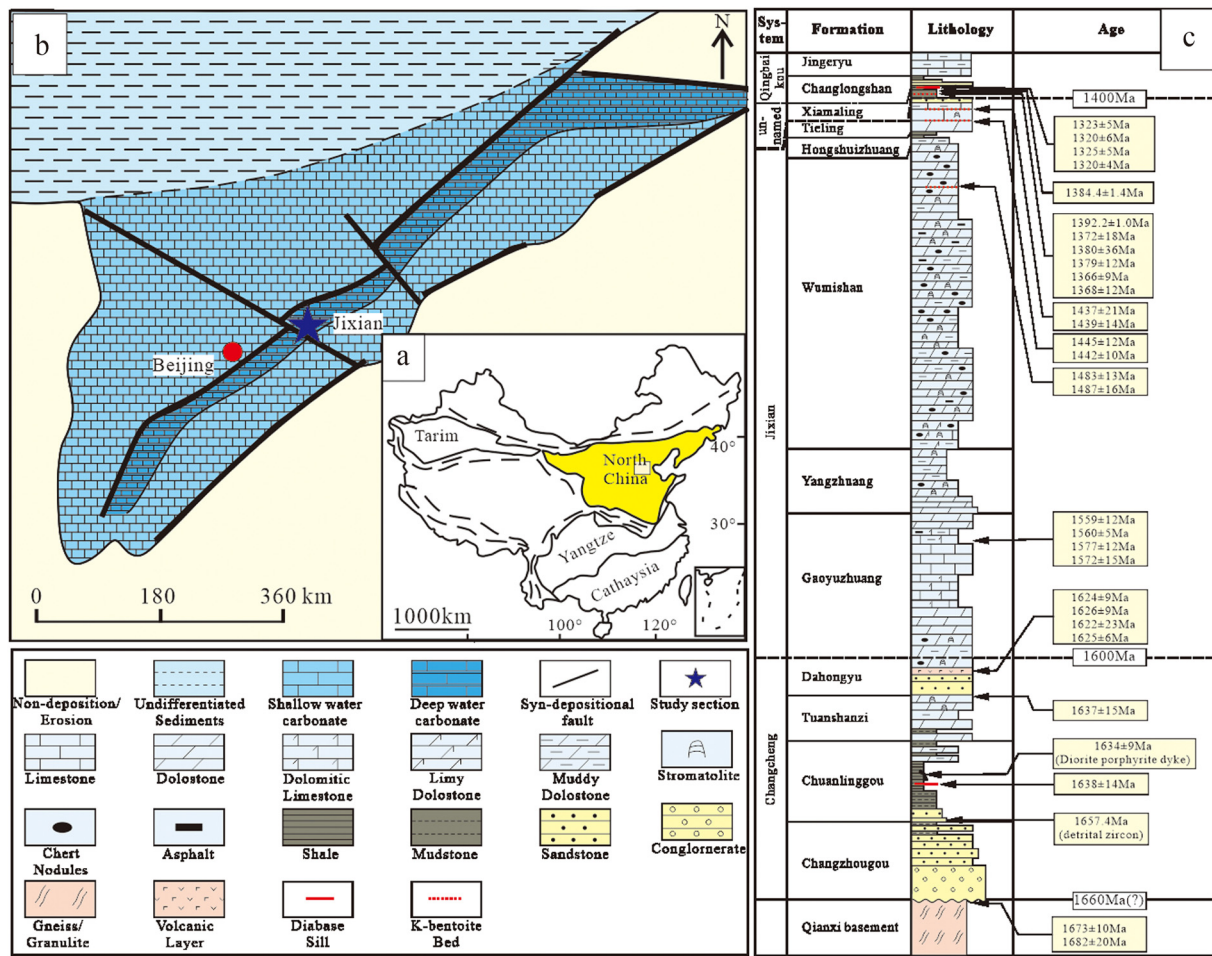


Fig. 1. a. Major tectonic units in China showing the position of the North China Craton; b. Paleogeographic map of the North China craton during the Mesoproterozoic era (modified after Wang et al., 2020). Blue star marks the location of the Jixian section; c. Late Paleo- to Neoproterozoic stratigraphic profile of the Yanliao basin (modified after Li et al., 2019, with age data from references therein). (For interpretation of the colours in the figure(s), the reader is referred to the web version of this article.)

3. Materials and methods

In this study, 71 outcrop samples were collected from the Gaoyuzhuang Formation in the type section of Jixian County (40.0439°N, 117.4008°E). Microscope images of representative samples are shown in the Supplementary Information (Fig. S1). Major and trace elements of all samples were analysed via X-ray fluorescence (XRF) using a Rigaku ZSX100e spectrometer and an Agilent Technologies 7700x quadrupole ICP-MS, respectively. Total organic carbon (TOC) concentrations were measured by combustion using a LECO CS-344 carbon-sulphur analyser (supplementary Table S1). Carbonate rocks that have not been subjected to deep burial dolomitization and have total Fe concentrations >0.5 wt% are considered suitable for palaeoredox interpretation via Fe speciation (Clarkson et al., 2014). In this study sixteen carbonate samples with FeT >0.5 wt% were chosen for iron speciation analysis, following the sequential extraction procedure of Poulton and Canfield (2005) (supplementary Table S2). Fifty samples with >50 ppb Mo were analysed for $\delta^{98}\text{Mo}$ using ^{97}Mo - ^{100}Mo double spike methods outlined in Li et al. (2014) and Zhao et al. (2015). The Mo isotopic ratios were determined on a Thermo-Fisher Scientific NeptunePlus multiple collector inductively coupled plasma mass spectrometer in the State Key Laboratory of Continental Dynamics, Northwest University. These fifty sample powders chosen for Mo isotopic analysis were also analysed for carbonate carbon ($\delta^{13}\text{C}_{\text{carb}}$) and oxygen ($\delta^{18}\text{O}$) isotopes by Continuous Flow-Isotope Ratio Mass Spectrometry (CF-IRMS) on a Europa Scientific 20-20

IRMS in Iso-Analytical Limited (supplementary Table S3). The Detailed analytical procedures are attached in on-line Supplementary information, Materials and methods.

4. Results

All new geochemical data are provided in the Supplementary Information (Table S1). Fig. 2 presents new and published (Zhang et al., 2018) data for the Jixian section in a stratigraphic and sedimentological framework, alongside changes in relative sea level based on interpreted facies (Mei, 2007). $\delta^{13}\text{C}_{\text{carb}}$ varies from -2.6‰ to $+0.4\text{‰}$, with three prominent negative excursions in the lower half of the succession, the lower two of which have not previously been documented (Fig. 2c). The first negative excursion is confined to a 2 m thick interval that transcends the flooding surface defining the boundary between members I and II, with values of $\delta^{13}\text{C}_{\text{carb}}$ decreasing from -0.5‰ to a nadir of -2.6‰ (Fig. 2c). The second negative excursion occurs in the lower part of Member III, where values steadily decrease from -0.6‰ to -1.9‰ as water depth increases to fair-weather wave base. The third excursion corresponds to the negative $\delta^{13}\text{C}_{\text{carb}}$ anomaly in the middle of Member III that has been correlated regionally in sections across the North China craton (e.g., Zhang et al., 2018). Samples from upper Member III and lower Member IV show some scatter in $\delta^{13}\text{C}_{\text{carb}}$ values between -0.9‰ and 0.0‰ (mean = -0.5‰), superimposed upon a gradual shift towards higher average $\delta^{13}\text{C}_{\text{carb}}$ up-section.

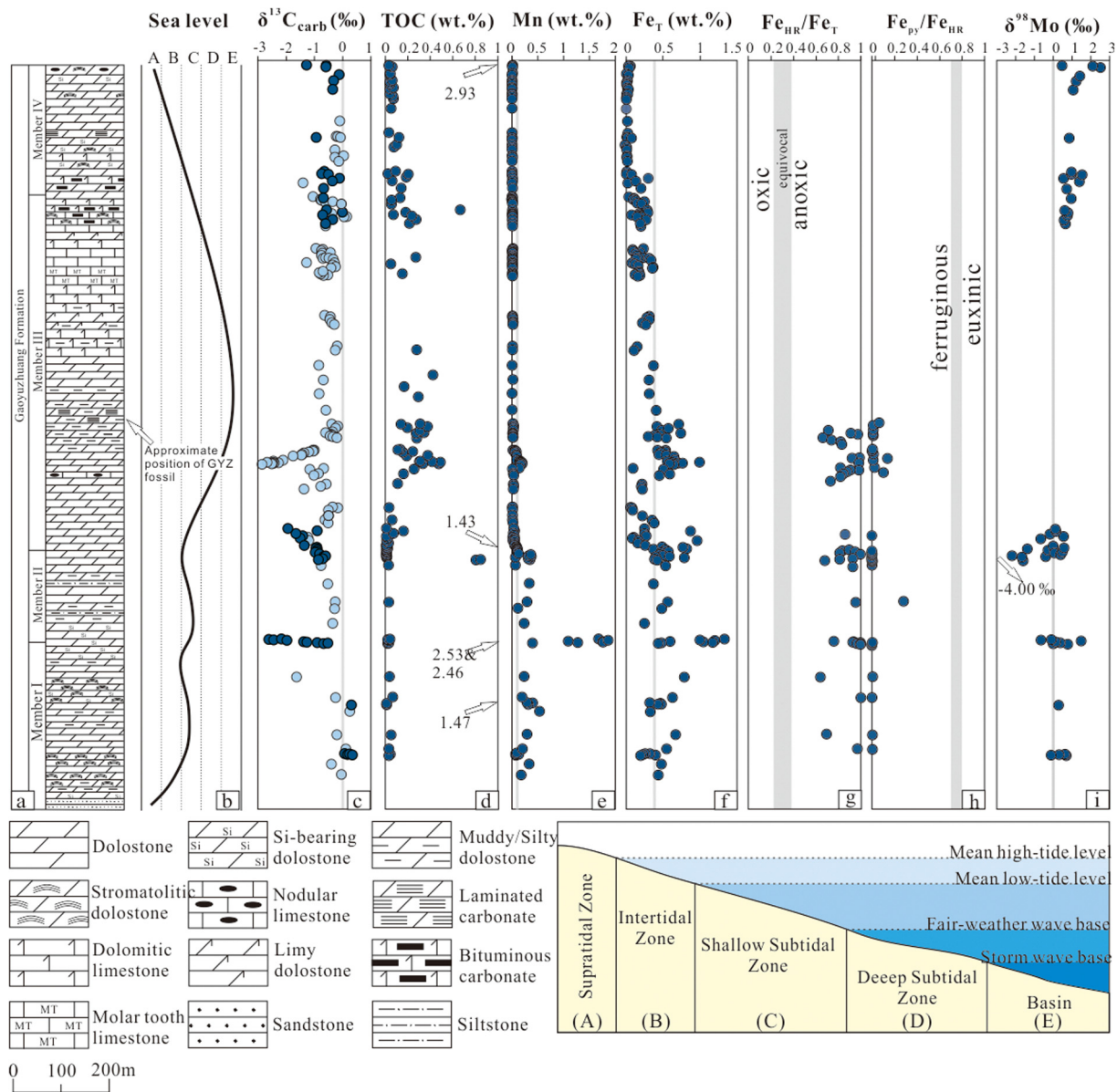


Fig. 2. Stratigraphic profile and geochemical data for the Gaoyuzhuang Formation at the Jixian section. Data presented are compiled from Zhang et al. (2018) in addition to new data in this study (Tables S1–S3). (a) Simplified stratigraphic profile of the Gaoyuzhuang Formation, showing the approximate level of the Gaoyuzhuang fossil horizon; (b) Simplified interpretation of relative sea level change based on sedimentary facies analysis; (c) $\delta^{13}\text{C}_{\text{carb}}$, data in pale blue are from Zhang et al. (2018); (d) TOC; (e) Mn; (f) Fe_T . Vertical lines in plots of total Mn (0.11 wt%) and Fe concentration (0.38 wt%) denote average carbonate concentrations for these elements (Turekian and Wedepohl, 1961); (g) $\text{Fe}_{\text{HR}}/\text{Fe}_T$ ratios; (h) $\text{Fe}_{\text{Py}}/\text{Fe}_{\text{HR}}$ ratios; (i) $\delta^{98}\text{Mo}_{\text{carb}}$ isotopic compositions.

Average TOC concentrations are generally low (mean = 0.2 wt%), with the exception of four muddy dolomite samples from members I and II, and one sample from Member IV, where concentrations are above 2 wt% (Fig. 2d). In members I and II, Mn and Fe_T (Fig. 2) are generally close to, or above, average carbonate compositions of 0.11 wt% for Mn and 0.38 wt% for Fe (Turekian and Wedepohl, 1961). A cluster of samples in the basal half of Member III have elevated Mn and Fe_T contents, corresponding to the oxygenation event outlined in previous studies (Zhang et al., 2018; Shang et al., 2019), but other samples in members III and IV are below average carbonate compositions, with a distinct overall decrease up-section. Specifically, in Member I, Mn and Fe_T concentrations range from 0.05–1.77 wt% (mean = 0.57 wt%) and 0.21–1.17 wt% (mean = 0.49 wt%), respectively. Both Mn and Fe_T rapidly increase across the transitional interval between members I and II, in tandem with the first negative $\delta^{13}\text{C}_{\text{carb}}$ excursion, to reach maximum concentrations of 2.42 wt% and 1.33 wt%, respectively,

before decreasing to moderately enriched values for the remainder of Member II (mean Mn = 0.22 wt%; mean Fe_T = 0.52 wt%, $n = 10$). Through members III and IV, short intervals of significant Fe_T (and muted Mn) enrichment (max Fe = 0.99 wt%, max Mn = 0.20 wt%) coincide with two prominent negative $\delta^{13}\text{C}_{\text{carb}}$ excursions in the lower – middle part of Member III, followed by gradually decreasing Fe_T and Mn up-section, coincident with an increase and stabilisation of $\delta^{13}\text{C}_{\text{carb}}$ at higher values. Mn and Fe_T decrease further in the upper part of Member III and remain stable throughout Member IV, around very low mean values of 11.3 ppm (5.2–25.8 ppm) for Mn and 0.03 wt% (from <0.01 to 0.08 wt%) for Fe_T .

The majority of carbonate samples analysed in this study have $\text{Fe}_T < 0.5$ wt% and were therefore not analysed for Fe speciation (Clarkson et al., 2014). However, 16 samples across the Member I – II, and II – III boundary intervals contain $\text{Fe}_T > 0.5$ wt%, and these samples were combined with previously published data (Zhang et al., 2018), together demonstrating significant enrichments in highly

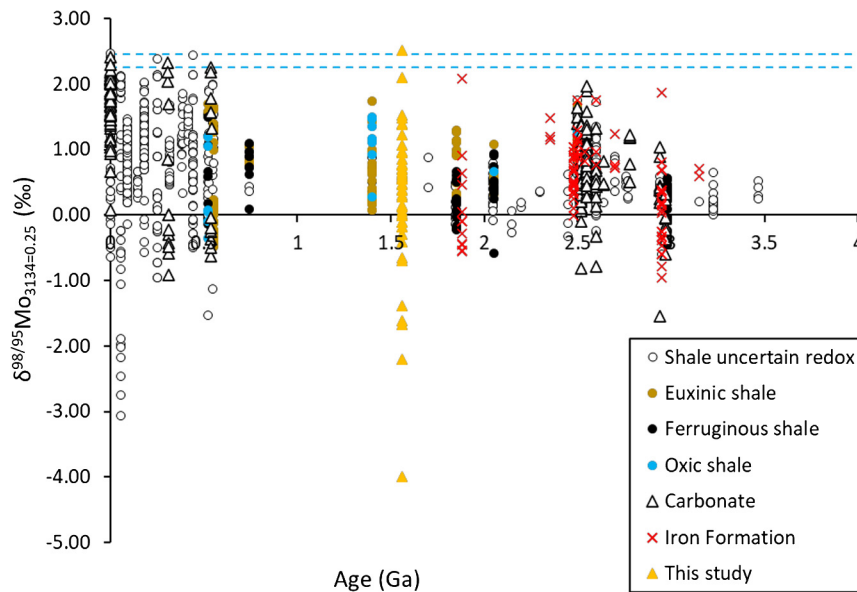


Fig. 3. Compilation of $\delta^{98}\text{Mo}$ through geological time (adapted after Thoby et al., 2019). Samples are colour coded to indicate local depositional redox conditions based on accompanying Fe speciation data where possible. Modern seawater $\delta^{98}\text{Mo}$ composition (and associated uncertainty) shown as blue horizontal dashed lines. Carbonate $\delta^{98}\text{Mo}$ data from this study are shown as orange triangles.

reactive iron ($\text{Fe}_{\text{HR}}/\text{Fe}_{\text{T}} > 0.38$) coupled with low $\text{Fe}_{\text{py}}/\text{Fe}_{\text{HR}}$ ratios (< 0.01 ; Fig. 2).

The Gaoyuzhuang Formation documents the largest range in $\delta^{98}\text{Mo}_{\text{carb}}$ recorded in the geological record to date (Figs. 2 and 3). Values for $\delta^{98}\text{Mo}_{\text{carb}}$ in the lower part of Member I show limited variability (mean = $0.36 \pm 0.32\text{‰}$, $n = 5$), with the range of values increasing at the boundary between members I and II ($\delta^{98}\text{Mo}_{\text{carb}} = -0.01$ to $+1.48\text{‰}$, mean = $0.25 \pm 0.64\text{‰}$, $n = 8$). The Member II – III boundary interval shows significant scatter in $\delta^{98}\text{Mo}_{\text{carb}}$, where highly negative values in the upper part of Member II (min = -4.00‰ , mean = $-0.60 \pm 1.22\text{‰}$, $n = 17$) gradually transition to higher values (max = 0.33‰) in the lower part of Member III. The $\delta^{98}\text{Mo}_{\text{carb}}$ compositions of samples from the upper part of Member III and through Member IV are markedly more elevated, with an apparent increasing trend from values initially around 0.6‰ to a maximum of 2.51‰ (mean = $1.05 \pm 0.54\text{‰}$, $n = 19$).

5. Discussion

5.1. Pulsed oxygenation events in the Yanliao Basin

Our data are consistent with previous palaeoredox datasets for the Gaoyuzhuang Formation that argue for deposition under redox-stratified water column conditions (Zhang et al., 2018; Shang et al., 2019; Wang et al., 2020). Specifically, $\text{Fe}_{\text{HR}}/\text{Fe}_{\text{T}} > 0.38$ and $\text{Fe}_{\text{py}}/\text{Fe}_{\text{HR}} < 0.7$ together indicate that deeper waters were anoxic and ferruginous in the Yanliao basin during deposition of members I and II, and in the lower part of Member III (Zhang et al., 2018). Short-lived enrichments in redox-sensitive trace elements (e.g., Mo, U) have been taken as evidence to suggest that some parts of the basin may have experienced transient euxinia during deposition of middle Member III (Wang et al., 2020). However, we find no evidence for euxinia in our Fe speciation analyses, and instead the high $\text{Fe}_{\text{HR}}/\text{Fe}_{\text{T}}$ (> 0.68) and low $\text{Fe}_{\text{py}}/\text{Fe}_{\text{HR}}$ (< 0.01) ratios suggest that the Gaoyuzhuang Formation was most likely deposited under dominantly ferruginous conditions. As such, limited Mo enrichment in 3 samples from shallow-marine facies to the north of the Jixian section (Wang et al., 2020) may more reasonably be interpreted to represent intermittent Mo drawdown in association with Fe and Mn (oxyhydr)oxides.

Zhang et al. (2018) combined Fe speciation analyses with REE data at the Jixian section and noted a distinct transition to more negative Ce anomalies coincident with a basin-wide negative $\delta^{13}\text{C}_{\text{carb}}$ excursion in the middle of Member III (Fig. 2). These authors suggest that the combined data represent a distinct water column oxygenation event that resulted in the widespread oxidation of deeper water ferrous iron, approximately coincident with the first appearance of decimetre-scale multicellular macrofossils in stratigraphic sections further to the east (Zhu et al., 2016; Zhang et al., 2018). Our $\delta^{13}\text{C}_{\text{carb}}$ data augments previously published data by providing a higher resolution reconstruction of lower parts of the succession, suggesting that the previously recorded oxygenation event was preceded by two earlier pulsed oxygenation events, at the boundary between members I and II, and in the lowermost part of Member III (Fig. 2). This is supported by elevated Mn and Fe drawdown (to varying degrees; Fig. 2), consistent with precipitation as (oxyhydr)oxide phases during upwelling of dissolved Fe and Mn into oxic shallower waters (Zhang et al., 2018).

It is also possible that periodic increases in the upwelling flux of dissolved Fe and Mn may have resulted in enhanced draw down of Mn and Fe (oxyhydr)oxide minerals. Under this scenario, the coincident negative $\delta^{13}\text{C}_{\text{carb}}$ excursions could potentially represent incorporation of light $\delta^{13}\text{C}$ into diagenetic Fe and Mn carbonates formed during the remineralisation of organic matter. However, as noted by Zhang et al. (2018), these intervals are specifically characterised by preservation of high proportions of Fe (oxyhydr)oxides, which contrasts with intervals between the $\delta^{13}\text{C}_{\text{carb}}$ excursions, where more extensive transformation of Fe (oxyhydr)oxides to Fe carbonates is apparent. Thus, while a contribution from periodic changes in the upwelling flux of dissolved Fe and Mn cannot be entirely discounted, enhanced oxygen production in surface waters was likely the dominant control on extensive Fe and Mn (oxyhydr)oxide deposition.

In addition, we note that each of the three $\delta^{13}\text{C}_{\text{carb}}$ excursions coincides with increasing water depth, but that as water depth further increased in each case, $\delta^{13}\text{C}_{\text{carb}}$ returns to heavier values (Fig. 2c). Thus, while short-term changes in water depth are difficult to determine with certainty, each of the excursions appears consistent with a deepening of the oxycline to a point, below which, the deeper waters remained anoxic. Furthermore, there is an apparent progressive increase in the maximum depth of the

oxycline with each subsequent oxygenation pulse, with the first pulse resulting in oxygenation into the shallow subtidal zone, the second pulse resulting in oxygenation to fair-weather wave base, and the third pulse oxygenating the water column to storm wave base. Thus, while oxygenation was restricted to relatively shallow waters, which is consistent with evidence from the Southern Urals (Doyle et al., 2018), each pulse progressively ventilated deeper waters.

In addition to documenting an oxygenation pulse in Member III, Zhang et al. (2018) proposed that the gradual increase in $\delta^{13}\text{C}_{\text{carb}}$ through the upper part of Member III and Member IV, in combination with consistently negative Ce/Ce^* throughout the interval, represents progressive water column oxygenation. However, a return to low $\text{I}/(\text{Ca}+\text{Mg})$ in shallow platform carbonates of upper Member III to the northwest of the Jixian section has been interpreted to support a return to low oxygen levels following the pulsed oxygenation event in the middle of Member III (Shang et al., 2019). Thus, uncertainty currently remains over the extent of oxygenation above the final observed oxygenation pulse in Member III. However, there is a progressive shallowing in water depth from the middle of Member III through Member IV (Fig. 2b), and thus the local redox indicators that have previously been applied to this part of the succession are limited in their ability to track the extent of oxygenation of deeper waters. Indeed, it is entirely possible that there were several additional pulses of oxygenation to progressively deeper depths after the final observed oxygenation pulse, but the signal of such pulses would only be recorded in deeper water sediments. Our major element and $\delta^{13}\text{C}_{\text{carb}}$ data are not inconsistent with continued oxygenation up-section, and certainly do not indicate a shoaling of the oxycline, since we see no evidence for either Mn or Fe drawdown, or significant $\delta^{13}\text{C}_{\text{carb}}$ excursions to lower values. However, further evaluation of the extent of ocean oxygenation after the observed oxygenation pulses requires consideration of a proxy that records a global signal, and in this regard we utilise Mo isotope systematics, as discussed below.

5.2. Evaluating the molybdenum isotope record of oxygenation

Accurate reconstruction of the molybdenum isotope composition of seawater ($\delta^{98}\text{Mo}_{\text{sw}}$) is the key requirement in paleoredox studies utilising Mo isotopes. Traditionally, Mo isotope studies have focused on shales, due to low Mo concentrations in carbonates, and uncertainties in isotopic fractionation during incorporation of Mo into the carbonate lattice and during diagenesis (Romaniello et al., 2016; Clarkson et al., 2020). However, recent studies suggest that the incorporation of seawater-derived molybdate into the carbonate lattice may be accompanied by negligible Mo isotopic fractionation in the absence of detrital impurities or pore-water sulfide production during diagenesis (Voegelin et al., 2010; Romaniello et al., 2016; Thoby et al., 2019). Testing the fidelity of carbonate samples to capture $\delta^{98}\text{Mo}_{\text{sw}}$ therefore demands strict screening criteria. In this regard, non-quantitative conversion of molybdate to tetrathiomolybdate, in addition to Mo adsorption onto Mn and Fe (oxyhydr)oxides, are two dominant pathways that may result in significant isotopic fractionation and preferential sedimentary retention of ^{95}Mo , resulting in sedimentary Mo isotopic compositions that are lower than contemporaneous $\delta^{98}\text{Mo}_{\text{sw}}$ (e.g., Siebert et al., 2003; Poulson Brucker et al., 2009). This is particularly significant during Mo adsorption onto Fe and Mn (oxyhydr)oxides, which results in isotopic fractionations of up to -3‰ relative to $\delta^{98}\text{Mo}_{\text{sw}}$ (Siebert et al., 2003; Goldberg et al., 2009; Poulson Brucker et al., 2009).

Samples from the lower Gaoyuzhuang Formation preserve amongst the most negative $\delta^{98}\text{Mo}$ values reported from the geological record (min = -4.00‰ ; Fig. 3). The $\delta^{98}\text{Mo}$ of the riverine

Mo input through geological time is poorly constrained, but is unlikely to have fallen below 0‰ (Dahl et al., 2010; Neubert et al., 2011). As such, the negative $\delta^{98}\text{Mo}_{\text{carb}}$ values recorded in the lower Gaoyuzhuang Formation record significant fractionations from seawater $\delta^{98}\text{Mo}$. Indeed, samples with particularly low $\delta^{98}\text{Mo}_{\text{carb}}$ compositions coincide with the three oxygenation pulses that initiated precipitation of highly elevated concentrations of Mn and Fe (Fig. 2, Table S1, S3). Thus, these fractionations would likely have been imparted through preferential adsorption of ^{95}Mo onto Fe and Mn (oxyhydr)oxides in the water column (Barling and Anbar, 2004; Goldberg et al., 2009). This Mo was then incorporated into the carbonate lattice as a result of recycling during early diagenesis (e.g., Poulson Brucker et al., 2009; Goldberg et al., 2012). In some instances, the $\delta^{98}\text{Mo}_{\text{carb}}$ composition was apparently altered further to give extremely light values, likely through repeated cycles of Fe and Mn reduction and re-oxidation in pore fluids. Thus, while these samples provide interesting insight into the genesis of exceptionally depleted $\delta^{98}\text{Mo}$ values in the marine carbonate record, they clearly do not reflect $\delta^{98}\text{Mo}_{\text{sw}}$.

In addition, however, our data from the lower part of the succession show that relatively high background concentrations of Mn and Fe are also common between the oxygenation pulses (Fig. 2, Table S1, S3), particularly in members I and II (where in contrast to the intervals with lower Mn and Fe in Member III, we have samples with coeval $\delta^{98}\text{Mo}_{\text{carb}}$ data). This is consistent with enhanced Fe and Mn precipitation under anoxic water column conditions, which may have been induced via a variety of processes, including (oxyhydr)oxide precipitation during anoxygenic photosynthesis (e.g., Crowe et al., 2008) or oxidation at the oxycline, potentially followed by transfer of such minerals to mixed ferrous/ferric phases such as green rust (which has a very high adsorptive capacity) during settling through the water column (Zegeye et al., 2012). Thus, significant Mo isotopic fractionation would also be expected for these samples, and we thus discount all samples from Members I and II, and the lower part of Member III, from our evaluation of $\delta^{98}\text{Mo}_{\text{sw}}$.

By contrast, some samples from the upper part of Member III and through Member IV may more faithfully record $\delta^{98}\text{Mo}_{\text{sw}}$. The screening criteria for these samples are shown in Fig. 4. Although deposited under oxic water column conditions, samples below a height of 1314 m have relatively high Fe and Mn contents, and these samples dominantly have higher Mo concentrations and light $\delta^{98}\text{Mo}_{\text{carb}}$ compositions, likely reflecting water column adsorption of Mo onto detrital Fe and Mn (oxyhydr)oxides during transport and deposition. Two samples from this zone have elevated $\delta^{98}\text{Mo}_{\text{carb}}$ compositions ($>1\text{‰}$), likely reflecting spatial separation in the later stage uptake of heavier $\delta^{98}\text{Mo}$ that remained in pore waters after initial recycling and re-adsorption of lighter $\delta^{98}\text{Mo}$. A relatively high detrital flux for these samples from upper Member III is supported by positive correlations between refractory elements (Al and Ti) and both Mn and Fe (Fig. 5). These samples also display negative correlations between $\delta^{98}\text{Mo}_{\text{carb}}$ and both Al and Ti (Fig. 5), which supports Mo fractionation during uptake by detrital Fe and Mn oxides.

Three samples from the top of the succession in Member IV also have high Mo concentrations and relatively high Mn concentrations (Fig. 4). These samples display a wide range in $\delta^{98}\text{Mo}_{\text{carb}}$, and have thus also likely been affected by recycling of adsorbed Mo. In addition, these three samples have relatively high Mg/Ca (Fig. 4), suggesting that they may have been affected by recrystallisation during dolomitization. However, as noted below, this does not appear to have adversely affected the $\delta^{98}\text{Mo}_{\text{carb}}$ composition of other samples from Member IV, and hence the dominant control on these three samples was likely diagenetic recycling of adsorbed Mo.

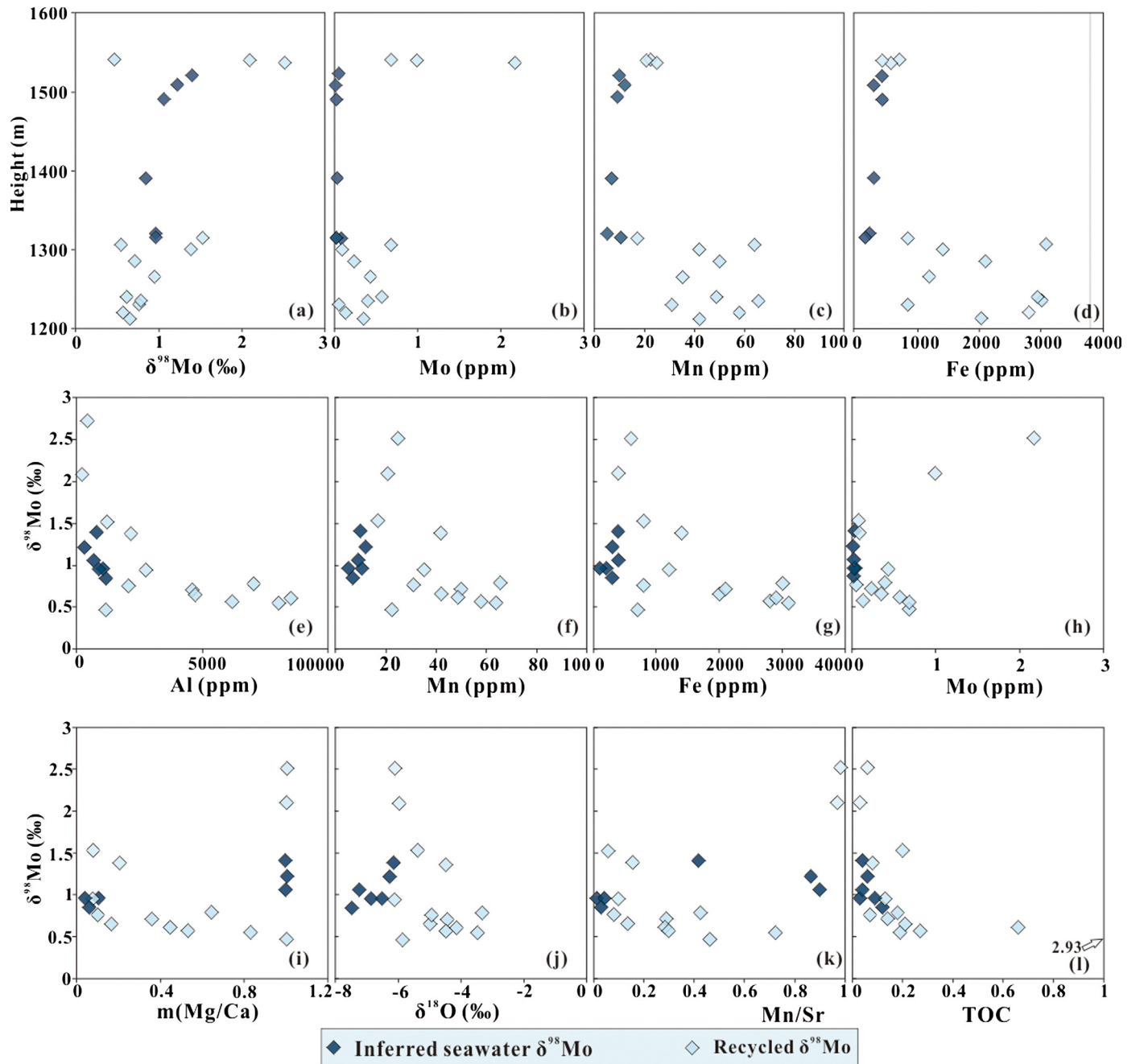


Fig. 4. Screening criteria used to determine carbonate samples that most faithfully record seawater $\delta^{98}\text{Mo}$ for samples from the upper Gaoyuzhuang Member III and Member IV. Depth profiles are shown for: a. $\delta^{98}\text{Mo}$ compositions, b. Mo concentrations, c. Mn concentrations, and d. Fe concentrations. Vertical lines on (c) and (d) represent average concentrations in carbonates for Mn and Fe, respectively (Turekian and Wedepohl, 1961). Cross plots are shown between $\delta^{98}\text{Mo}$ and e. Al, f. Mn, g. Fe, h. Mo, i. $m(\text{Mg}/\text{Ca})$, j. $\delta^{18}\text{O}$, k. Mn/Sr, and l. TOC.

The remaining samples from Member IV are characterised by low Fe, Mn and Mo concentrations, with no significant correlations between $\delta^{98}\text{Mo}_{\text{carb}}$ and either Mn, Fe or TOC (Fig. 4). We also observe no correlation between $\delta^{98}\text{Mo}_{\text{carb}}$ and Mg/Ca, implying negligible fractionation associated with recrystallisation during the minor degree of dolomitization that some of these samples have experienced. In addition, limited open-system elemental and isotopic exchange during diagenesis is supported by generally low Mn/Sr ratios (<1) and $\delta^{18}\text{O}_{\text{carb}}$ compositions ($> -8\text{‰}$) (Fig. 4), which is consistent with the reported preservation of normal marine REE signatures (Zhang et al., 2018). We therefore consider that these remaining samples from Member IV provide the best estimate of $\delta^{98}\text{Mo}_{\text{SW}}$, which gives a range of 0.85–1.41‰.

5.3. Constraining the global redox state of the ocean at ~1540 Ma

To constrain the global redox state of the ocean during deposition of the upper Gaoyuzhuang sediments, we build a single reservoir Mo cycling model with a fixed river input and three sinks for oxic, reducing non-euxinic (i.e., ferruginous) and euxinic conditions. The isotope composition of the marine Mo reservoir is tracked, and all isotope fractionation effects are fixed (see Table 1). Sinks are allowed to vary in size as a function of the area of seafloor characterised by each redox state, the marine Mo concentration, and an ‘offshore scaling’ (OSS) which assumes that reducing and euxinic sinks will require progressively more seafloor area as they expand into areas with lower C_{org} fluxes

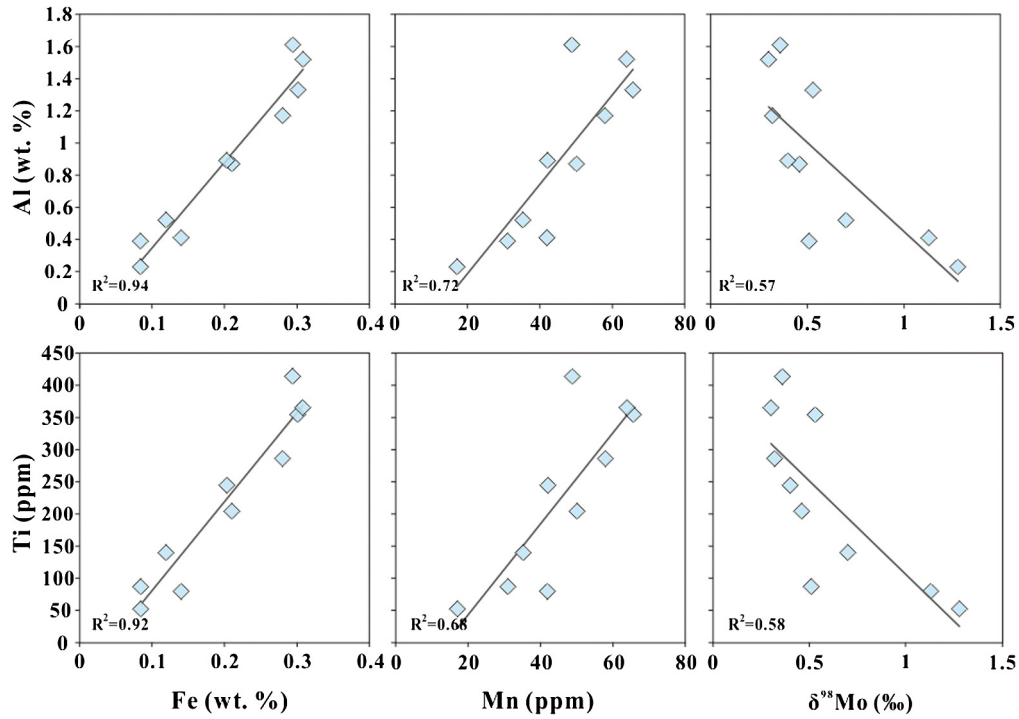


Fig. 5. Cross plots showing relationships between Fe, Mn and $\delta^{98}\text{Mo}_{\text{carb}}$ as a function of both Al and Ti.

Table 1

Marine Mo isotope mass balance model equations.

Name	Equation
Present day ocean Mo	$[\text{Mo}]_0 = 1.35 \times 10^{14} \text{ mol}$
Present day ocean $\delta^{98}\text{Mo}$	$\delta^{98}\text{Mo}_{\text{sw0}} = 2.37\text{‰}$
Area fraction for reducing sink	$A_{\text{reducing0}} = 0.015$
Area fraction for euxinic sink	$A_{\text{euxinic0}} = 0.0005$
Area fraction for oxic sink	$A_{\text{oxic0}} = 1 - A_{\text{reducing0}} - A_{\text{euxinic0}}$
Present day riverine Mo input	$K_{\text{input}} = 30 \times 10^7 \text{ mol yr}^{-1}$
Present day burial via oxic sink	$K_{\text{oxicburial}} = 8.7 \times 10^7 \text{ mol yr}^{-1}$
Present day burial via reducing sink	$K_{\text{reducingburial}} = 19.4 \times 10^7 \text{ mol yr}^{-1}$
Present day burial via euxinic sink	$K_{\text{euxinicburial}} = 1.9 \times 10^7 \text{ mol yr}^{-1}$
Fractionation effect: reducing sink	$\Delta_{\text{reducing}} = 1\text{‰}$
Fractionation effect: oxic sink	$\Delta_{\text{oxic}} = 3\text{‰}$
$\delta^{98}\text{Mo}$ of riverine flux	$\delta^{98}\text{Mo}_{\text{input}} = 0.55\text{‰}$
Fixed riverine input flux	$F_{\text{input}} = K_{\text{input}}$
Oxic sink burial flux	$F_{\text{oxic}} = K_{\text{oxicburial}} \cdot \left(\frac{A_{\text{oxic}}}{A_{\text{oxic0}}} \right) \cdot \left(\frac{[\text{Mo}]}{[\text{Mo}]_0} \right)$
Reducing sink burial flux	$F_{\text{reducing}} = K_{\text{reducingburial}} \cdot \left(\frac{A_{\text{reducing}}}{A_{\text{reducing0}}} \right) \cdot \left(\frac{[\text{Mo}]}{[\text{Mo}]_0} \right) \cdot \text{OSS}_r$
Euxinic burial sink flux	$F_{\text{euxinic}} = K_{\text{euxinicburial}} \cdot \left(\frac{A_{\text{euxinic}}}{A_{\text{euxinic0}}} \right) \cdot \left(\frac{[\text{Mo}]}{[\text{Mo}]_0} \right) \cdot \text{OSS}_e$
Seawater Mo mass balance	$\frac{d([\text{Mo}])}{dt} = F_{\text{input}} - F_{\text{oxic}} - F_{\text{reducing}} - F_{\text{euxinic}}$
Seawater Mo isotope mass balance	$\frac{d([\text{Mo}] \cdot \delta^{98}\text{Mo})}{dt} = F_{\text{input}} \cdot \delta^{98}\text{Mo}_{\text{input}} - F_{\text{oxic}} \cdot (\delta^{98}\text{Mo}_{\text{sw}} - \Delta_{\text{oxic}}) - F_{\text{reducing}} \cdot (\delta^{98}\text{Mo}_{\text{sw}} - \Delta_{\text{reducing}}) - F_{\text{euxinic}} \cdot \delta^{98}\text{Mo}_{\text{sw}}$

(Reinhard et al., 2013). We ran the model 100,000 times from a present day initialisation under random choices of reducing and euxinic area fractions, to create a map of the system $[\text{Mo}]$ and $\delta^{98}\text{Mo}$ response at steady state, under the initial conditions outlined in Table 1 (which also includes flux and reservoir calculations).

We use an updated database of published Mo concentration data from shales that are independently constrained to have been deposited under euxinic water column conditions to derive the best estimate of Mesoproterozoic seawater $[\text{Mo}]$ concentration. This approach is consistent with previous methods for $[\text{Mo}]$ estimation (e.g., Scott et al., 2008; Reinhard et al., 2013) and relies upon the assumption that, under euxinic conditions, $\text{H}_2\text{S}_{\text{aq}}$ is sufficiently elevated to permit near-quantitative Mo drawdown to sediments. The updated database yields a sediment $[\text{Mo}]$ range of 6–34 ppm (representing the central 75% of Mesoproterozoic eu-

xinic shale values), which is consistent with previous estimates derived from late Paleo- to Neoproterozoic euxinic shales (mean = 24 ppm, Scott et al., 2008; Reinhard et al., 2013). Scaling this with observed ratios between Mo concentration in open marine euxinic shales and homogeneous seawater Mo concentration (~ 105 nM) in the modern ocean, yields a value of ~ 21 nM for Mesoproterozoic seawater $[\text{Mo}]$. The $\delta^{98}\text{Mo}_{\text{carb}}$ composition of screened samples from the Gaoyuzhuang Formation is 0.85–1.41‰, which as discussed above is assumed to best represent $\delta^{98}\text{Mo}_{\text{sw}}$. In Fig. 6 we plot only the model outputs that fall within the above ranges for $\delta^{98}\text{Mo}_{\text{sw}}$ and $[\text{Mo}]$.

The model results suggest that to satisfy our estimated ranges for $\delta^{98}\text{Mo}_{\text{sw}}$ and $[\text{Mo}]$, a lower limit of $\sim 30\%$ of the seafloor had sufficient oxygen to result in the Mo isotopic fractionation associated with adsorption onto Mn and Fe (oxyhydr)oxides. While this is a lower limit in the model, we did not test all of the param-

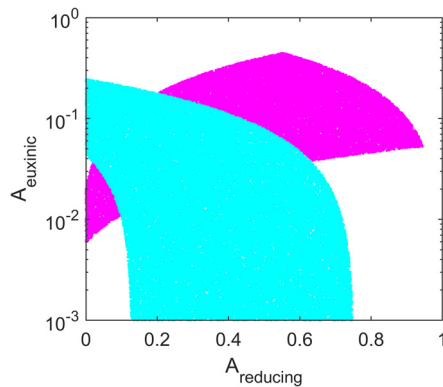


Fig. 6. Results of the isotope mass balance for carbonate samples that most likely represent the $\delta^{98}\text{Mo}_{\text{sw}}$ composition. Model output satisfying $6.45 \leq [\text{Mo}] \leq 34.4$ (blue) and $0.85 \leq \delta^{98}\text{Mo} \leq 1.41$ (pink). These map to a range of reducing and euxinic seafloor areas but exclude combined reducing and euxinic areas of more than 70% of the seafloor. Thus, oxic seafloor area is constrained to be 30% or more.

ter ranges associated with the system (e.g. the flux of riverine Mo or its isotopic composition), so values below 30% remain possible. Of the anoxic seafloor, the model suggests dominantly ferruginous waters, with around 1–10% of the ocean floor being subject to euxinia, which is consistent with current views on the stratified redox nature of the Mesoproterozoic ocean (Planavsky et al., 2011; Poulton and Canfield, 2011; Doyle et al., 2018). To evaluate whether these upper Gaoyuzhuang Formation samples reflect additional oxygenation after the final deeper water oxygenation pulse observed in the lower part of Member III (see above), we consider here the approximate range in seafloor area that was likely bathed in waters to the depth of storm wave base (since this represents the deepest depth of oxygenation observed during the three oxygenation pulses). Modern global relief models (Amante and Eakins, 2009) suggest that storm wave base currently encompasses less than 5% of the global seafloor. Thus, notwithstanding possible differences in this value through time, our suggestion of ~30% seafloor oxygenation in the upper Gaoyuzhuang Formation is significantly larger than the ~5% seafloor oxygenation indicated lower in the succession. This supports continued progressive oxygenation of deeper waters (Zhang et al., 2018), to a depth that likely extended into parts of the deep ocean, after the final observed oxygenation pulse in Member III of the Gaoyuzhuang Formation.

While this study provides a snapshot into the extent of global ocean oxygenation in the early Mesoproterozoic, we stress that the long-term trajectory of oceanic oxygenation across this Era remains unclear. Indeed, it is not known whether the Gaoyuzhuang Formation documents a temporally-restricted rise in the extent of oceanic oxygenation, or whether the oxygenation we observe represents the initial stages of more persistent oxygenation that ultimately resulted in the possible development of OMZ-type conditions by ~1.4 Ga (Zhang et al., 2016, 2019). What is clear, however, is that the Mesoproterozoic was actually a rather dynamic interval that certainly experienced significant variability in the extent of ocean oxygenation, whether it be fluctuating or progressive, and this likely had major implications for macroevolutionary dynamics that we are only just beginning to unravel (e.g., Zhang et al., 2018).

6. Conclusions

Our combined evaluation of $\delta^{13}\text{C}_{\text{carb}}$, iron-speciation systematics, and Fe_T and Mn data support pulsed oxygenation events in the early Mesoproterozoic ocean at ~1.56 Ga. These pulsed events led to progressive longer-term oxygenation of shallower waters, while the deeper ocean remained anoxic and ferruginous. Mo isotope measurements in Gaoyuzhuang Formation samples provide a

means to estimate the global extent of oxygenation at this time. Samples deposited during periods of intense Fe and Mn (oxyhydr)oxide precipitation record the lowest $\delta^{98}\text{Mo}$ compositions observed in the geological record, due to isotopic fractionation during adsorption to oxide minerals and subsequent recycling during diagenesis. However, following a careful screening procedure which eliminated samples that have experienced a significant authigenic or diagenetic overprint, a $\delta^{98}\text{Mo}_{\text{sw}}$ value of 0.85–1.41‰ was obtained. A single reservoir Mo cycling model was then utilised, combining a refined estimate of seawater $[\text{Mo}]$ with our $\delta^{98}\text{Mo}_{\text{sw}}$ value, to suggest that at least 30% of the global seafloor was bathed beneath an oxic water column during deposition of the shallow-water upper Gaoyuzhuang Formation. Since this value encapsulates far more of the ocean floor than is covered down to a depth of storm wave base (the deepest depth for which there is direct evidence for oxygenation further down the Gaoyuzhuang Formation), this implies a progressive deepening of the oxycline through the upper Gaoyuzhuang Formation. Our data thus suggest significant, progressive oxygenation dynamics, which occurred in the form of temporally-restricted pulses, during the early Mesoproterozoic. It remains unclear whether the oxygenation we observe represents the initiation of longer-term enhanced oxygenation through the Mesoproterozoic, or a protracted interval of anomalously high levels of oxygenation coincident with the evolution of decimetrescale, multicellular eukaryotes.

CRedit authorship contribution statement

Jin Luo: Data curation, Investigation, Visualization, Writing – original draft. **Xiaoping Long:** Conceptualization, Supervision, Writing – review & editing. **Fred T. Bowyer:** Visualization, Writing – review & editing. **Benjamin J.W. Mills:** Methodology. **Jie Li:** Methodology. **Yijun Xiong:** Investigation. **Xiangkun Zhu:** Resources. **Kan Zhang:** Resources. **Simon W. Poulton:** Conceptualization, Writing – review & editing.

Declaration of competing interest

The authors declare that they have no known competing financial interests or personal relationships that could have appeared to influence the work reported in this paper.

Acknowledgements

Thanks are given to Bin Wu, Xi Zhu, Jingyu Wang and Yilin Gao for their assistance in fieldwork. We also thank Bingshuang Zhao and Xi Zhu for their help with analyses. This study was supported by the National Natural Science Foundation of China (41890831) and the National Key Research and Development Project of China (2020YFA0714803). SWP, BJWM and FB were funded by NERC (NE/R010129/1). SWP acknowledges support from a Royal Society Wolfson Research Merit Award, and XZ acknowledges support from China Geological Survey (DD20190002). We thank Andrey Bekker and Phil Fralick for helpful comments on the manuscript.

Appendix A. Supplementary material

Supplementary material related to this article can be found online at <https://doi.org/10.1016/j.epsl.2021.116754>.

References

- Amante, C., Eakins, B.W., 2009. ETOP01 1 Arc-Minute Global Relief Model: Procedures, Data Sources and Analysis 24. NOAA Technical Memorandum NESDIS NGDC, 19 pp.
- Asael, D., Rouxel, O., Poulton, S.W., Lyons, T.W., Bekker, A., 2018. Molybdenum record from black shales indicates oscillating atmospheric oxygen levels in the early Paleoproterozoic. *Am. J. Sci.* 318, 275–299.

- Barling, J., Anbar, A.D., 2004. Molybdenum isotope fractionation during adsorption by manganese oxides. *Earth Planet. Sci. Lett.* 217, 315–329.
- Beghin, J., Guilbaud, R., Poulton, S.W., Gueneli, N., Brocks, J.J., Storme, J., Blanpied, C., Javaux, E.J., 2017. A palaeoecological model for the late Mesoproterozoic – early Neoproterozoic Atar/El Mreïti Group, Taoudeni basin, Mauritania, northwestern Africa. *Precambrian Res.* 299, 1–14.
- Buick, R., Des Marais, D.J., Knoll, A.H., 1995. Stable isotopic compositions of carbonates from the Mesoproterozoic Bangemall group, northwestern Australia. *Chem. Geol.* 123, 153–171.
- Canfield, D.E., Zhang, S., Frank, A.B., Wang, X., Wang, H., Su, J., Ye, Y.T., Frei, R., 2018. Highly fractionated chromium isotopes in Mesoproterozoic-aged shales and atmospheric oxygen. *Nat. Commun.* 9, 2871.
- Chen, J.B., Zhuang, H.M., Xing, Y.S., Ma, G.G., 1981. On the Upper Precambrian (Sinian Suberathem) in China. *Precambrian Res.* 15, 207–228.
- Chu, X.L., Zhang, T.G., Zhang, Q.R., Lyons, T.W., 2007. Sulfur and carbon isotope records from 1700 to 800 Ma carbonates of the Jixian section, northern China: implications for secular isotope variations in Proterozoic seawater and relationships to global supercontinental events. *Geochim. Cosmochim. Acta* 71, 4668–4692.
- Clarkson, M.O., Poulton, S.W., Guilbaud, R., Wood, R.A., 2014. Assessing the utility of Fe/Al and Fe-speciation to record water column redox conditions in carbonate-rich sediments. *Chem. Geol.* 382, 111–122.
- Clarkson, M.O., Musing, K., Andersen, M.B., Derek, V., 2020. Examining pelagic carbonate-rich sediments as an archive for authigenic uranium and molybdenum isotopes using reductive cleaning and leaching experiments. *Chem. Geol.* 539, 199412.
- Cole, D.B., Reinhard, C.T., Wang, X.L., Gueguen, B., Halverson, G.P., Gibson, T., Hodgskiss, M.S.W., McKenzie, N.R., Lyons, T.W., Planavsky, N.J., 2016. A shale-hosted Cr isotope record of low atmospheric oxygen during the Proterozoic. *Geology* 44, 555–558.
- Crowe, S.A., Jones, C., Katsev, S., Magen, C., O'Neill, A.H., Sturm, A., Canfield, D.E., Haffner, G.D., Mucci, A., Sundby, B., Fowle, D.A., 2008. Photoferrotrophs thrive in an Archean ocean analogue. *Proc. Natl. Acad. Sci. USA* 105, 15,938–15,943.
- Dahl, T.W., Hammarlund, E.U., Anbar, A.D., Bond, D.P.G., Gill, B.C., Gordon, G.W., Knoll, A.H., Nielsen, A.T., Schovsbo, N.H., Canfield, D.E., 2010. Devonian rise in atmospheric oxygen correlated to the radiations of terrestrial plants and large predatory fish. *Proc. Natl. Acad. Sci. USA* 107, 17911–17915.
- Doyle, K.A., Poulton, S.W., Newton, R.J., Podkovyrov, V.N., Bekker, A., 2018. Shallow water anoxia in the Mesoproterozoic ocean: evidence from the Bashkir Megan-ticlinorium, Southern Urals. *Precambrian Res.* 317, 196–210.
- Gilleaudeau, G.J., Kah, L.C., 2013. Carbon isotope records in a Mesoproterozoic epicratonic sea: carbon cycling in a low-oxygen world. *Precambrian Res.* 228, 85–101.
- Goldberg, T., Archer, C., Vance, D., Poulton, S.W., 2009. Mo isotope fractionation during adsorption to Fe (oxyhydr)oxides. *Geochim. Cosmochim. Acta* 73, 6502–6516.
- Goldberg, T., Archer, C., Vance, D., Thamdrup, B., McAnena, A., Poulton, S.W., 2012. Controls on Mo isotope fractionations in a Mn-rich anoxic marine sediment, Gullmar Fjord, Sweden. *Chem. Geol.* 296–297, 73–82.
- Guo, H., Du, Y.S., Kah, L.C., Huang, J.H., Hu, C.Y., Huang, H., Yu, W.C., 2013. Isotopic composition of organic and inorganic carbon from the Mesoproterozoic Jixian Group, North China: implications for biological and oceanic evolution. *Precambrian Res.* 224, 169–183.
- Javaux, Lepot, 2018. The Paleoproterozoic fossil record: implications for the evolution of the biosphere during Earth's middle-age. *Earth-Sci. Rev.* 176, 68–86.
- Kendall, B., Gordon, G.W., Poulton, S.W., Anbar, A.D., 2011. Molybdenum isotope constraints on the extent of late Paleoproterozoic ocean euxinia. *Earth Planet. Sci. Lett.* 307, 450–460.
- Li, H.K., Zhu, S.X., Xiang, Z.Q., Su, W.B., Lu, S.N., Zhou, H.Y., Geng, J.Z., Li, S., Yang, F.J., 2010. Zircon U-Pb dating on tuff bed from Gaoyuzhuang Formation in Yan-qing Beijing: further constraints on the new subdivision of the Mesoproterozoic stratigraphy in the northern North China Craton. *Acta Petrol. Sin.* 26, 2131–2140.
- Li, J., Liang, X.R., Zhong, L.F., Wang, X.C., Ren, Z.Y., Sun, S.L., Zhang, Z.F., Xu, J.F., 2014. Measurement of the isotopic composition of molybdenum in geological samples by MC-ICP-MS using a novel chromatographic extraction technique. *Geostand. Geoanal. Res.* 38, 345–354.
- Li, S.Z., Li, X.Y., Wang, G.Z., Liu, Y.M., Cheng, W.Z., Wang, T.S., Cao, X.Z., Yu, G.X., Somerville, I., Li, Yang, Zhou, J., Dai, L.M., Jiang, S.H., Zhao, H., Wang, Y., Wang, G., Yu, S., 2019. Global Mesoproterozoic plate reconstruction and formation mechanism for Precambrian basins: constraints from three cratons in China. *Earth-Sci. Rev.* 198, 102946.
- Lu, S.N., Zhao, G.C., Wang, H.C., Hao, G.J., 2008. Precambrian metamorphic basement and sedimentary cover of the North China Craton: a review. *Precambrian Res.* 160, 77–93.
- Mei, M.X., 2007. Sedimentary features and their implication for the depositional succession of non-stromatolitic carbonates, Mesoproterozoic Gaoyuzhuang Formation in Yanshan area of North China. *Geoscience* 21, 45–56 (in Chinese with English abstract).
- Morford, J.L., Emerson, S., 1999. The geochemistry of redox sensitive trace metals in sediments. *Geochim. Cosmochim. Acta* 63, 1735–1750.
- Neubert, N., Heri, A.R., Voegelin, A.R., Nägler, T.F., Schlunegger, F., Villa, I.M., 2011. The molybdenum isotopic composition in river water: constraints from small catchments. *Earth Planet. Sci. Lett.* 304, 180–190.
- Planavsky, N.J., McGoldrick, P., Clinton, T.S., Li, C., Reinhard, C.T., Kelly, A.E., Chu, X.L., Bekker, A., Love, G.D., Lyons, T.W., 2011. Widespread iron-rich conditions in the mid-Proterozoic ocean. *Nature* 477, 448.
- Planavsky, N.J., Slack, J.F., Cannon, W.F., O'Connell, B., Isson, T.T., Asael, D., Jackson, J.C., Hardisty, D.S., Lyons, T.W., Bekker, A., 2018. Evidence for episodic oxygenation in a weakly redox-buffered deep mid-Proterozoic ocean. *Chem. Geol.* 483, 581–594.
- Poulton, S.W., Canfield, D.E., 2005. Development of a sequential extraction procedure for iron: implications for iron partitioning in continentally derived particulates. *Chem. Geol.* 214, 209–221.
- Poulton, S.W., Canfield, D.E., 2011. Ferruginous conditions: a dominant feature of the ocean through Earth's history. *Elements* 7, 107–112.
- Reinhard, C.T., Planavsky, N.J., Robbins, L.J., Partin, C.A., Gill, B.C., Lalonde, S.V., Bekker, A., Konhauser, K.O., Lyons, T.W., 2013. Proterozoic ocean redox and biogeochemical status. *Proc. Natl. Acad. Sci. USA* 110, 5357–5362.
- Romaniello, S.J., Herrmann, A.D., Anbar, A.D., 2016. Syndepositional diagenetic control of molybdenum isotope variations in carbonate sediments from the Bahamas. *Chem. Geol.* 438, 84–90.
- Scott, C., Lyons, T.W., Bekker, A., Shen, Y., Poulton, S.W., Chu, X.L., Anbar, A.D., 2008. Tracing the stepwise oxygenation of the Proterozoic ocean. *Nature* 452, 456–459.
- Shang, M.H., Tang, D.J., Shi, X.Y., Zhou, L.M., Zhou, X.Q., Song, H.Y., Jiang, G.Q., 2019. A pulse of oxygen increase in the early Mesoproterozoic ocean at ca. 1.57–1.56 Ga. *Earth Planet. Sci. Lett.* 527, 115797.
- Siebert, C., Nagler, T.F., Blanckenburg, F.V., Kramers, J.D., 2003. Molybdenum isotope records as a potential new proxy for paleoceanography. *Earth Planet. Sci. Lett.* 211, 159–171.
- Slack, J.F., Grenne, T., Bekker, A., Rouxel, O.J., Lindberg, P.A., 2007. Suboxic deep sea-water in the late Paleoproterozoic: evidence from hematitic chert and iron formation related to seafloor-hydrothermal sulfide deposits, central Arizona, USA. *Earth Planet. Sci. Lett.* 255, 243–256.
- Slack, J.F., Cannon, W.F., 2009. Extraterrestrial demise of banded iron formations 1.85 billion years ago. *Geology* 37, 1011–1014.
- Thoby, M., Konhauser, K.O., Fralick, P.W., Altermann, W., Visscher, P.T., Lalonde, S.V., 2019. Global importance of oxic molybdenum sinks prior to 2.6 Ga revealed by the Mo isotope composition of Precambrian carbonates. *Geology* 47, 559–562.
- Tian, H., Zhang, J., Li, H.K., Su, W.B., Zhou, H.Y., Yang, L.G., Xiang, Z.Q., Geng, J.Z., Liu, H., Zhu, S.X., Xu, Z.X., 2015. Zircon LA-MC-ICP-MS U-Pb dating of tuff from Mesoproterozoic Gaoyuzhuang Formation in Jixian County of North China and its geological significance. *Acta Geosci. Sin.* 36, 647–658.
- Turekian, K.K., Wedepohl, K.H., 1961. Distribution of the elements in some major units of the Earth's crust. *Geol. Soc. Am. Bull.* 72, 175–192.
- Voegelin, A.R., Nagler, T.F., Beukes, N., Lacassie, J.P., 2010. Molybdenum isotopes in late Archean carbonate rocks: implications for early Earth oxygenation. *Precambrian Res.* 182, 70–82.
- Wang, Z.P., Wang, X.Q., Shi, X.Y., Tang, D.J., Stüeken, E.E., Song, H.Y., 2020. Coupled nitrate and phosphate availability facilitated the expansion of eukaryotic life at ca. 1.56 Ga. *J. Geophys. Res., Biogeosci.* 125, e2019JG005487.
- Zegeye, A., Bonneville, S., Benning, L.G., Sturm, A., Fowle, D.A., Jones, C., Canfield, D.E., Ruby, C., MacLean, L.C., Nomosatryo, S., Crowe, S.A., Poulton, S.W., 2012. Green rust formation controls nutrient availability in a ferruginous water column. *Geology* 40, 599–602.
- Zhang, K., Zhu, X.K., Wood, R.A., Shi, Y., Gao, Z.F., Poulton, S.W., 2018. Oxygenation of the Mesoproterozoic ocean and the evolution of complex eukaryotes. *Nat. Geosci.* 11, 1110–1120.
- Zhang, S.C., Wang, X.M., Wang, H.J., Bjerrum, C.J., Hammarlund, E.U., Costa, M.M., Connelly, J.N., Zhao, B.M., Su, J., Canfield, D.E., 2016. Sufficient oxygen for animal respiration 1,400 million years ago. *Proc. Natl. Acad. Sci. USA*, 201523449.
- Zhang, S.C., Wang, X.M., Wang, H.J., Bjerrum, C.J., Hammarlund, E.U., Haxen, E.R., Wen, H.J., Ye, Y.T., Canfield, D.E., 2019. Paleoenvironmental proxies and what the Xiamaling Formation tells us about the mid-Proterozoic ocean. *Geobiology* 17, 225–246.
- Zhao, P.P., Li, J., Zhang, L., Wang, Z.B., Kong, D.X., Ma, J.L., Wei, G.J., Xu, J.F., 2015. Molybdenum mass fractions and isotopic compositions of international geological reference materials. *Geostand. Geoanal. Res.* 40, 217–226.
- Zhu, S.X., Zhu, M.Y., Knoll, A.H., Yin, Z.J., Zhao, F.C., Sun, S.F., Qu, Y.G., Shi, M., Liu, H., 2016. Decimetre-scale multicellular eukaryotes from the 1.56-billion-year-old Gaoyuzhuang Formation in North China. *Nat. Commun.* 7, 1–8.